Chemical Engineering Journal 411 (2021) 128472

Contents lists available at ScienceDirect

Chemical Engineering Journal

journal homepage: www.elsevier.com/locate/cej

Hydrophobic eutectic solvents: Thermophysical study and application in removal of pharmaceutical products from water

Fernando Bergua [a,c], Miguel Castro [b,d], José Muñoz-Embid [a,c], Carlos Lafuente [a,c], Manuela Artal [a,c,*]

[a] Departamento de Química Física, Facultad de Ciencias, Universidad de Zaragoza, Zaragoza, Spain
[b] Departamento de Ciencia y Tecnología de Materiales y Fluidos, Universidad de Zaragoza, Zaragoza, Spain
[c] Instituto Agroalimentario de Aragón – IA2 (Universidad de Zaragoza – CITA), Zaragoza, Spain
[d] Instituto de Nanociencia y Materiales de Aragón (INMA), Universidad de Zaragoza - CSIC, Zaragoza, Spain

ARTICLE INFO

Keywords:
Thymol
Carboxylic acid
Eutectic
Emerging contaminants
Thermophysical properties
Solubility and extraction

ABSTRACT

Exposure to persistent contaminants presents a risk to humans and animals. Specifically, the occurrence of drugs in aqueous ecosystems is related to the increase in antimicrobial resistance. Several methods to remove them have been studied but most have cost and toxicity drawbacks. Thus, the study of new eco-sustainable procedures is needed as the liquid–liquid extraction with hydrophobic solvents (ESs). In this study, we prepared six ESs mixtures with thymol (Thy) and octanoic acid (Oct) or decanoic acid (Dec) and evaluated their extractive ability in aqueous mixtures of quercetin (*Q*), nitrofurantoin (*NF*), or tetracycline (*TC*). In addition, we measured, correlated, and modelled both the solid–liquid equilibria of the two systems and seven thermophysical properties of the mixtures. From these calculations, we obtained the melting enthalpies of the eutectic points, isobaric thermal expansibilities, intermolecular free lengths, orientational dipolar parameters, thermodynamic properties of the surface, critical temperatures, and activation energies of viscous flow. The perturbed chain statistical associating fluid theory was found to be suitable for predicting the thermodynamic behaviour of these systems. Next, we determined the solubility of the three drugs both in water and in the eutectic mixtures, as well as the efficiency extraction (*EE*) of the latter. We obtained the highest extraction efficiency for the equimolar [Thy:Oct] mixture, which was the most polar solvent. The values were: $EE(Q) = 97.8\%$, $EE(NF) = 84.9\%$, and $EE(TC) = 95.0\%$. Further, performing the procedure with three cycles increased these values above 99%. The results showed the highest hydrophobicity for quercetin and the lowest for nitrofurantoin.

1. Introduction

The pharmaceutical industry has an unquestionable impact on the world economy. According to data collected by the European statistical agency Eurostat [1], €36,500 million was invested in R&D in this sector in 2018. Moreover, 765,000 directly related jobs and four times more indirectly were generated. Currently, even for essential drugs, consumption exceeds need, as deduced from the different values listed for OECD countries [2]. In 2017, Turkey showed the lowest consumption of substances for the treatment of cardiovascular diseases (C, code ATC) have a defined daily dosage (DDD) per 1000 inhabitants of 176.4. In contrast, Hungary was the largest consumer, having a DDD of 722.2. However, each Turkish consumer consumed antibiotics (J01, code ATC) for 13 days/year whereas, for a Dutch consumer, this value was only 3.5 days/year. In addition, figures related to the pharmaceutical market for veterinary use are also important. More than 6700 tons of antimicrobials for food-producing animals were sold in 2017 [3], half of them in the Mediterranean area, which is an especially vulnerable ecosystem [4] because of the low water renewal rate. The inappropriate management of drug production and human and animal waste have resulted in the appearance of these compounds in the environment, for example, soil and residual water [5]. Note that 30–90% of the oral dose of the most of the active substances are excreted. As a result, both humans and animals suffer involuntary exposure to antimicrobial compounds, which contributes to increase resistance to antimicrobial infections (AMR). Currently, it is estimated that the AMR causes approximately 700,000 deaths per year, and this number will increase to 10 million by 2050 if no action is taken [6]. In addition to antibiotics, a wide variety of

* Corresponding author at: Departamento de Química Física, Facultad de Ciencias, Universidad de Zaragoza, Zaragoza, Spain.
E-mail address: martal@unizar.es (M. Artal).

https://doi.org/10.1016/j.cej.2021.128472
Received 25 November 2020; Received in revised form 23 December 2020; Accepted 6 January 2021
Available online 12 January 2021

pharmaceutical and personal care products (PPCPs) have been found in the environment, including hormones, anti-inflammatory, antiepileptic, and repellent compounds [7–9]. These compounds are considered emerging contaminants and described as "pseudo-persistent" pollutants [10]. Although their detected concentrations are small, they reach a steady state in the environment, so continuous exposure increases the risks of AMR [11,12]. In fact, AMR is an emerging problem that requires urgent control according to the World Health Organization [13].

In water treatment plants, raw water is processed in three stages: (i) clarification (coagulation, flocculation, and sand filtration), (ii) refining (such as adsorption on activated carbon, membrane filtration, and oxidation processes), and (iii) disinfection (ozonation/chlorination/ultraviolet). The first step results in the elimination of solids and organic material, but it has little effect on the micropollutant contents [11,12]. The efficiency of the remaining steps depends on many factors including the physicochemical properties of the contaminants, their possible interaction with other components (chemical or biological) in the wastewater, and properties (for example, composition and size) of the retention system [13–15]. Adsorption using activated carbon is a simple and inexpensive practice, but it can present problems related to degradation and saturation with the organic matter in the water. Alternative adsorbent, such as graphene, graphene oxide and carbon nanotubes, have been proposed but their high cost has prevented their implementation [16]. Furthermore, the presence of microparticles from the adsorbents could have a toxic effect on aquatic microorganisms [14,17]. Biological treatment with both cultures and activated sludge has a highly variable efficiency that depends on the enzymatic induction capacity of the bacteria, as well as the operating conditions and the physicochemical properties of the contaminants. For example, compounds such as tetracycline and carbamazepine are very resistant to biodegradation, and increases in their concentration have been detected after treatment [14]. Finally, chemical processes as ozonation, fenton oxidation, UV or ionizing radiation treatment have shown effectiveness but have drawbacks related to the length of the process and its cost, as well as the toxicity of the obtained by-products [14,18]. Therefore, no existing process shows a clear advantage over the others; thus, several methods should be combined and new techniques should be developed [14,19]. Recently, the liquid–liquid extraction with deep eutectic solvents (DESs), eco-friendly mixtures with low transition temperatures, has emerged as a suitable procedure. Other extractants such as common organic solvents and ionic liquids have disadvantages related to their high toxicity and solubility in water [20,21]. In 2003, DESs were defined as mixtures that exhibit a decrease in melting temperature with respect to pure compounds by more than 100 °C, and a classification based on the mixture composition was proposed [22,23]. Types I, II, and IV contain metal salts or hydrated metal salts combined with organic salts or hydrogen bond donors. Type III includes a mixture of an organic salt (typically, an ammonium halide) and metabolites acting as hydrogen bond acceptors and donors, respectively. They are often called natural eutectics (NADESs) and have low toxicities [24]. These solvents are prepared by mixing, no chemical reaction, so their preparation is simple, economical, does not generate waste by-products, and is 100% efficient. All of these characteristics are essential principles of the '*green chemistry*'. In NADESs, small amounts of water are usually added as a modulating component because their very high viscosities. The marked hydrophilic character allows the use of NADES in several fields such as energy storage and biomass transformation, as well as solvents and catalysts in esterification reactions and adsorbents for the elimination of sulphur and nitrogen compounds in fuel mixtures and CO_2, SO_2, or N_2 for carbon capture and storage (CCS) technology [25–29].

In our research group, we have carried out thermophysical and spectroscopic studies of different type III DESs [30–35]. However, some applications may require solvents with higher hydrophobic character than those previously studied. In 2015, Van Osch et al. [36] studied the first hydrophobic DES by combining quaternary salts with decanoic acid. Subsequently, mixtures formed of neutral natural compounds such as menthol, thymol, and carboxylic acids were evaluated [37–45]. These non-ionic eutectics have weak intermolecular interactions, so no significant decrease in the melting point is observed. Thus, we prefer to use the term eutectic solvents (ESs) to refer to these mixtures, although several authors have classified them as type V DESs [38]. ESs have shown high efficiency in extraction processes in aqueous media because of their low viscosities, which facilitate mass transfer between phases, as well as their immiscibility with water [39,41–43,45]. To predict and establish the optimal technological conditions for processes involving ESs, knowledge of the solid–liquid phase diagram and the values of different properties such as density, surface tension, and compressibility are necessary. Recently, there has been a considerable increase in the interest of the scientific community in these solvents; however, in 2019, only 6% of the papers in this area focused on the physicochemical characterisation (Fig. S1). Specifically, we found only one study [44] that reported thermophysical data at several temperatures for the systems studied in this work: thymol + octanoic acid ([Thy:Oct]) and thymol + decanoic acid ([Thy:Dec]). Thus, we will be able to perform a quantitative comparison of the solid–liquid equilibrium (SLE) of both systems, as well as for the density and viscosity of an equimolar mixture with decanoic acid. Li et al. [45] also published the melting point and the density and viscosity at 298.15 K for equimolar mixtures of both systems.

Thymol is a monoterpenoid that is widely used in the agro-food industry to avoid the growth of microorganisms in cosmetics and pharmaceuticals because of its antibacterial and antifungal activity. In addition, its use as a flavouring compound is well-known [46]. Octanoic and decanoic acids are two middle chain fatty acids used as surfactants to make emulsions, gels, or coats, especially in the biotechnological field [47,48]. Owing to their appropriate thermal properties, they are also used as phase change materials (PCMs) [49,50]. Concerning the use of mixtures of these compounds for decontamination processes, Sas et al. [41] reported the removal of phenolic pollutants from water, Li et al. [45] analysed the microextraction of several fluoroquinolones, and Sereshti et al. [51] extracted tetracyclines from milk. Moreover, Wei et al. [52] studied the adsorption of PPCPs by combining hydrophilic DESs and metal–organic framework adsorbents. However, our work is the first study of the solubility of quercetin (*Q*), a flavonoid used in animal feed having pharmacological applications, nitrofurantoin (*NF*), antibiotic used to treat mild urinary tract infections, and tetracycline (*TC*), a broad-spectrum antibiotic, in thymol-based ESs and their subsequent removal from residual water. All of these compounds are poorly soluble in aqueous systems.

The final goal of this study was to evaluate the ability of different hydrophobic thymol-based eutectic mixtures (Thy-based ESs) to extract pharmaceutical products from contaminated water. Nevertheless, a comprehensive physicochemical characterisation of the solvents is required. First, the temperature range in which these systems remain liquid was determined. In addition, seven thermodynamic and transport properties at several temperatures were measured to analyse the thermophysical behaviour of these systems. The perturbed chain statistical associating fluid theory (PC-SAFT) equation of state (EoS) was used to model both the solid–liquid equilibrium and some thermodynamic properties. Finally, the solubility (at $T = 298.15$ K) of the three drugs in the water and the Thy-based ES systems as well as the extraction efficiency of the latter were analysed.

2. Materials and methods

2.1. Materials

Information about the chemicals used in this work is listed in Table S1 and Fig. 1. The compounds were supplied by Sigma–Aldrich and used without further purification. The studied Thy-based ES systems were Thy and Oct or Dec acid mixtures in molar ratios of 1:2, 1:1, and 2:1. They were prepared by mixing the components and subsequent

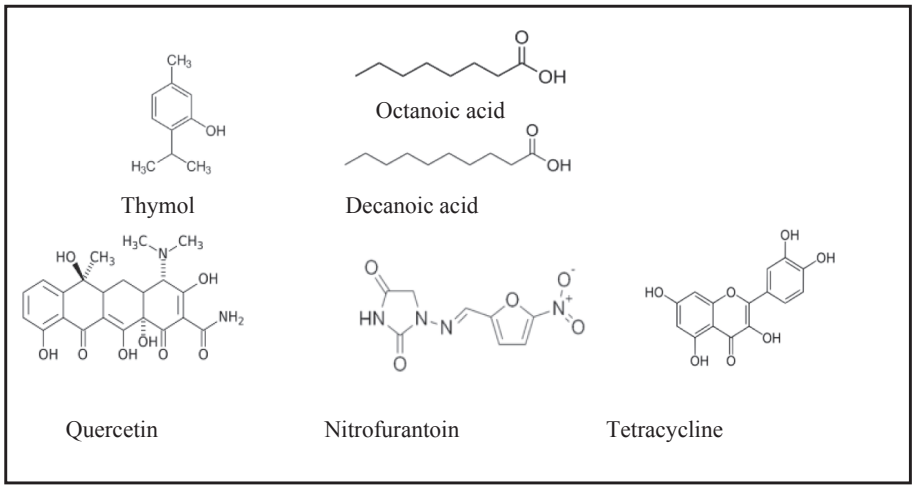

Fig. 1. Structure of the compounds used in this study.

heating at a moderate temperature (323 K) with magnetic stirring until a homogeneous liquid was formed. A PB210S Sartorius balance was used to weigh several compounds in adequate proportions. The uncertainty of the mass determination was 1×10^{-4} g. Table S2 reports the characteristics of the Thy-based ESs and acronyms used in this study including the molar ratio, molar mass (M) calculated from the molar ratio of each component, and the melting temperature (T_m) measured in this work for each mixture.

2.2. Thermophysical properties

Several different pieces of apparatus were used to measure the thermophysical properties of the prepared mixtures. Each piece of equipment was thermostatically controlled and checked by measuring the properties of benzene (greater than 99.5% purity). Table 1 lists the standard uncertainty in the temperature ($u(T)$) for each device, the calculated combined expanded uncertainties ($U_c(Y)$) for each property (0.95 level of confidence, k= 2), and the mean relative deviations ($MRD(Y)$) in comparison with the literature data for benzene [53]. To verify the accuracy of the T_m measurements, the corresponding values for pure Thy, Oct, and Dec are listed in Table S1.

2.3. Solubility and extraction experiments

The solubility (W) of the *Q*, *NF*, and *TC* in water and in the hydrophobic eutectic solvents was determined at 298.15 K by the shake-flask method. Three temperature controlled flasks protected from light degradation with aluminium foil were used and the solute was added in each flask up to super saturation and kept under stirring for 24 h. Afterwards sedimentation, three aliquots of each flask were centrifuged and filtered (PES syringe filter, 0.22 μm). Each result is the average value of nine analyses. The concentration was determined by UV–VIS spectroscopy with a double-beam spectrum VWR 6300 PC ($u(\lambda) = \pm 0.2$ nm). For each pharmaceutical compound, a calibration curve to quantify the mass fraction of the dissolved solute was constructed (Table S3). In the extraction experiments, three stock solutions of contaminated water with small quantities of *Q*, *NF*, or *TC* were prepared and their concentrations (C_i) were determined by UV–VIS as above mentioned. Similar volumes of this matrix (V_i) and the eutectic solvent (V_{DES}) was vigorously mixing during 24 h at T = 298.15 K. A sample of the aqueous phase was collected, centrifuged, filtered (PES syringe filter, 0.22 μm) and analysed. The composition of each drug (C_f) was calculated with the corresponding calibration curve (Table S3). In this case, we performed six analyses for each result and they were calculated as extraction efficiency ($EE = 100(C_i - C_f/C_i)$).

Table 1
Summary of the devices used in the measurement of the experimental properties.

Property	Devices	$u(T)$/K	$U_c(Y)$	$MRD(Y)$/%
ρ	Oscillating U-tube density meter Anton Paar DSA 5000	0.005	0.05 kg·m^{-3}	0.004
u	Oscillating U-tube density meter Anton Paar DSA 5000	0.005	0.5 m·s^{-1}	0.026
SLE,$C_{p,m}$	Differential scanning calorimeter TA Instruments DSC Q2000	0.01	0.5 K, 1%	0.028
n_D	Abbemat-HP refractometer Dr. Kernchen	0.01	2·10^{-5}	0.007
ε	Agilent 4263BA LCR 2 MHz	0.01	0.02	0.11
γ	Drop volume tensiometer Lauda TVT-2	0.01	1%	0.21
ν	Capillary viscosimeter Ubbelohde	0.01	1%	0.28

$$MRD(Y) = \frac{100}{n}\sum_{i=1}^{n}\left|\frac{Y_{i,lit} - Y_{i,exp}}{Y_{i,exp}}\right|.$$

2.4. Modelling

In this section, we present a brief description of the non-random two-liquid (NRTL) model and the PC-SAFT equation of state. For a more comprehensive description, the reader is directed to the literature [54–56].

2.4.1. NRTL

The difference between the interaction energy of a molecule with similar molecules and with those of the other molecules causes the local concentration around a molecule in a mixture to be different from that in the bulk. The NRTL model uses this concept to describe the relationship between the activity coefficient of the solute and the composition to correlate the phase equilibria. For a binary mixture:

$$\ln\gamma_1 = x_2^2\left[\frac{\tau_{21}G_{21}^2}{(x_1 + x_2G_{21})^2} + \frac{\tau_{12}G_{12}}{(x_2 + x_1G_{12})^2}\right] \quad (1)$$

$$G_{ij} = \exp\left(-\alpha A_{ij}/RT\right) \quad (2)$$

where x_i is the mole fraction of the component, i, and T is the temperature. The parameter α is a measure of the non-randomness of the solution; in this work, α = 0.3. The difference in energies between the i and j surfaces or cross-interaction energies, $A_{ij} = \left(g_{ij} - g_{ji}\right)$, are the pa-

rameters of the model, and they are obtained from the correlation of the phase equilibria data.

2.4.2. PC-SAFT EoS

In this model, the dimensionless Helmholtz energy (a) is given as the sum of the ideal gas contribution (a^{id}) and the residual one (a^{res}). This latter is calculated using perturbation theory. The repulsive interactions are included in the reference system (hard-chain fluid), whereas the attractive ones are considered a disturbance to the model. Thus,

$$a^{res} = a^{hc} + a^{dis} + a^{assoc} + a^{polar} \tag{3}$$

here a^{hc}, a^{dis}, a^{assoc} and a^{polar} represent the hard-chain, dispersive, association, and multipole contributions, respectively. In this work, the multipole term was not considered. The a^{hc} expression is taken from the approach of Chapman [57]. It depends on the chain segment number (m), on the radial pair distribution function of the segments (g^{hs}), and on the Helmholtz energy of the hard sphere system (a^{hs}):

$$a^{hc} = ma^{hs} - (m-1)\ln g^{hs} \tag{4}$$

The dispersive contribution is given as the sum of first-order and second-order terms, and it is calculated using the theory of Barker and Henderson extended to chain molecules [58,59]:

$$a^{dis} = -2\pi\rho m^2\left(\frac{\varepsilon}{kT}\right)\sigma^3 I_1 - \pi\rho mkT\left(\frac{\partial\rho}{\partial p}\right)_{hc} m^2\left(\frac{\varepsilon}{kT}\right)^2\sigma^3 I_2 \tag{5}$$

where ρ is the density, p is the pressure, T is the temperature, and σ, and ε are the segment diameter and segment energy, respectively. The perturbation integrals (I_1 and I_2) are replaced for a power series of sixth order in the segment number and in the packing fraction (η).

$$I_1(m,\eta) = \sum_{i=0}^{6}\left[a_{0i} + \frac{m-1}{m}a_{1i} + \frac{m-1}{m}\frac{m-2}{m}a_{2i}\right]\eta^i \tag{6}$$

$$I_2(m,\eta) = \sum_{i=0}^{6}\left[b_{0i} + \frac{m-1}{m}b_{1i} + \frac{m-1}{m}\frac{m-2}{m}b_{2i}\right]\eta^i \tag{7}$$

The parameters $a_{0i}, a_{1i}, a_{2i}, b_{0i}, b_{1i}$, and b_{2i} are called *universal model constants* and were obtained from the optimisation of the thermodynamic properties of *n*-alkanes (methane to *n*-decane). The three geometrical parameters needed to characterise each pure compound (m, σ, and ε) are calculated from thermodynamic data, mostly density and vapor pressures.

Finally, the association term is calculated from the fraction of unbonded monomers (X^A), which is related to the tendency to form *n*-mers (Δ), and the number of associated sites of the compound (S). The equations are as follows:

$$a^{assoc} = \sum_A\left[\ln X^A - \frac{X^A}{2}\right] + \frac{1}{2}S \tag{8}$$

$$X^A = \frac{1}{1+\rho X^A\Delta} \tag{9}$$

$$\Delta = \kappa^{A_iB_i}\sigma^3 g^{hs}\left[\exp\left(\frac{\varepsilon^{A_iB_i}}{kT}\right) - 1\right] \tag{10}$$

where $\kappa^{A_iB_i}$ is the association volume and $\varepsilon^{A_iB_i}$ is the association energy. The values of both parameters are necessary if the compound is an associated substance. For the mixtures, several mixing rules can be used. We estimated the mixing geometric parameters and those of association as $\sigma_{ij} = (\sigma_i + \sigma_j)/2$, $\varepsilon_{ij} = \sqrt{\varepsilon_i\varepsilon_j}(1-k_{ij})$, $\kappa^{A_iB_j} = \sqrt{\kappa^{A_iB_i}\kappa^{A_jB_j}}$, and $\varepsilon^{A_iB_j} = (\varepsilon^{A_iB_i} + \varepsilon^{A_jB_j})/2$. The subscripts i and j refer to each of the compounds present in the mixture, and k_{ij} is the binary interaction parameter sometimes required to correct the dispersion term of unlike molecules. It is usually obtained by fitting the experimental properties of the mixtures and, consequently, the model loses the predictive character. Herein, we performed a full predictive calculation ($k_{ij} = 0$) using the pure compound parameters (Table S4) as published by Martins et al. [44].

3. Results and discussion

3.1. Solid-liquid equilibria of [Thy]ESs

Knowledge of the phase behaviour of fluids is essential for their use as solvents in industrial applications. For eutectic mixtures, the experimental SLE diagram is required to determine whether predictive thermodynamic tools are suitable, and these tools may be viable alternative if they have been previously validated. The solid–liquid phase change of [Thy:Oct] and [Thy:Dec] systems was determined and the results were correlated with the NRTL model. The melting temperatures assuming ideal behaviour were calculated to quantify the non-ideality of these systems. In addition, the corresponding diagrams with the PC-SAFT equation of state were obtained to validate this EoS as a prediction tool for the phase behaviour of the Thy-based ESs. The experimental and calculated data are listed in Tables S5 and S6, and they are displayed in Fig. 2. The liquid window of [Thy:Oct] was higher than that for [Thy:Dec]. At $T \leq 298.15$ K, the first system was liquid at compositions (x_{Thy}, thymol mole fraction) of $0 < x_{Thy} < 0.60$, whereas that for the system with decanoic acid was $0.17 < x_{Thy} < 0.59$. In addition, the composition of the eutectic point (x^E_{Thy}) shifted to higher values as the chain length in the carboxylic acid increased. Table 2 lists the parameters for the correlation T_m versus x_{Thy} NRTL as well as the deviations obtained, which are within the experimental uncertainty. Our data for both systems agree with those published by Martins et al. [42], as shown in Fig. 2, except for the [Thy:Oct] system at $x_{Thy} > x^E_{Thy}$. For these compositions, the temperatures measured by us were higher. Moreover, the values measured by Li et al. [45] for the equimolar compositions (264.8 K for [Thy:Oct] and 284.6 K for [Thy:Dec]) were much lower than ours and those of Martins et al. [44]. Using the Tammann plots, we estimated the melting enthalpies of the eutectic points of our systems: 113.1 ± 1 J/g for [Thy:Oct] and 135.8 ± 1 J/g for [Thy:Dec]. Other PCMs such as pure fatty acids and their eutectic mixtures have more suitable (higher) values, but they also have higher melting temperatures, which can cause problems in some applications [49]. The range of the melting temperature of the Thy-based ESs, 20–32 °C, is ideal for use in building cooling. A comprehensive study of these mixtures as PCMs would include chemical stability, kinetics, and economic aspects, but this is outside the scope of this work.

For systems with simple eutectic diagrams, the solubility of the solid in the liquid phase can be calculated by the following thermodynamic relationship [60]:

$$\ln(x_i\gamma_i^l) = \frac{\Delta_m H_i}{R}\left(\frac{1}{T_{m,i}} - \frac{1}{T_m}\right) + \frac{\Delta_m C_{p,i}}{R}\left(\frac{T_{m,i}}{T_m} - \ln\frac{T_{m,i}}{T_m} - 1\right) \tag{11}$$

where γ_i^l is the activity coefficient in the liquid phase of component i at composition x_i;$T_{m,i}$ and $\Delta_m H_i$ are the melting temperature (K) and melting enthalpy (J·mol^{-1}), respectively, of component i;T_m is the melting temperature (K) of the mixture; and $\Delta_m C_{p,i}$ is the variation of the heat capacity of component i in the liquid and solid phases. Eq. (11) requires that the pure solids do not exhibit polymorphism and are independently crystallised. In addition, the second term is usually neglected because the variation of the heat capacities is much lower than the enthalpy contents. Thus, we calculated the solubilities assuming ideal behaviour ($\gamma_i^l = 1$). Both studied systems showed a negative deviation of the ideality (Fig. 2) but very small depressions of the eutectic temperature ($T^E_{exp} - T^E_{id}$): −2.4 for [Thy:Oct] and −5.3 K for [Thy:Dec]. This result indicates the presence of weak dispersive interactions between the hydrophobic groups of both components of each mixture.

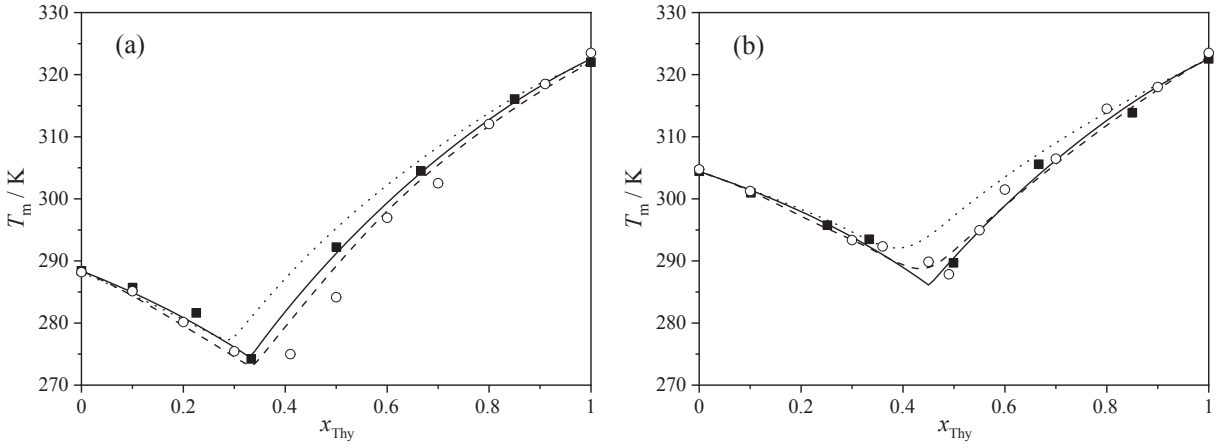

Fig. 2. Solid-liquid equilibria of the Thy-based ESs: (a) [Thy:Oct]; (b) [Thy:Dec] (■), This work; (○), Ref. [44]; (——), Ideal; (—), NRTL; (– –) PC-SAFT EoS. For reference, an additional line at$T$ = 298.15 K is included.

Table 2
NRTL correlation parameters and deviations in the melting temperature of the [Thy]ESs systems.

System	A_{12}/J·mol^{-1}	A_{21}/J·mol^{-1}	$AAD(T_m)$/K	$MRD(T_m)$/%
[Thy:Oct]	−3545.93	3579.20	0.9	0.25
[Thy:Dec]	−3776.02	3896.05	1.0	0.31

$$AAD(Y) = \frac{1}{n}\sum_{i=1}^{n}\left|Y_{i,calc} - Y_{i,exp}\right|$$

$$MRD(Y) = \frac{100}{n}\sum_{i=1}^{n}\left|\frac{Y_{i,calc} - Y_{i,exp}}{Y_{i,exp}}\right|.$$

Furthermore, we calculated γ_i^l $\left(\gamma_i^l = \varphi_i/\varphi_i^0\right)$ as the ratio between the fugacity coefficients of component i in the mixture (φ_i) and in the pure state (φ_i^0), both obtained with the PC-SAFT EoS. Fig. 2 and Table S5 show very good agreement between the experimental values and those obtained with PC-SAFT EoS. The mean relative deviations are listed in Table S7, and the average calculated for the mixtures containing octanoic or decanoic acid were$\overline{MRD}(T_m)$ = 0.44 and 0.31%, respectively.

3.2. Thermophysical study of [Thy]ESs

Thermophysical data are necessary for the optimisation of industrial processes. To characterise our thymol-based eutectic solvents at p = 0.1 MPa, the density (ρ), speed of sound (u), isobaric molar heat capacity ($C_{p,m}$), refraction index (n_D), static permittivity (ε), surface tension (γ), and kinematic viscosity (ν) of mixtures of [Thy:Oct] and [Thy:Dec] were measured. The compositions were close to the eutectic ratio: that is, molar ratios of (1:2), (1:1), and (2:1). The lower operating temperature was different accounting for the solid transition of each mixture and the upper was always 338.15 K. Tables S8 and S9 collect the experimental data at each T and composition and Table 3 lists the values at T = 298.15 and 313.15 K for each mixture to facilitate the reading of the paper. Usually, most thermodynamic properties exhibit a linear correlation with temperature. Here, the properties adjusted linearly are $\rho, u, C_{p,m}, n_D$, and γ, and Table 4 reports the fitted parameters.

The densities of both systems are lower than that of water in the

Table 3
Summary of the thermophysical properties at$p$ = 0.1 MPa of the studied [Thy]ESs mixtures.

		[Thy:Oct]			[Thy:Dec]		
Property	T/K	(1:2)	(1:1)	(2:1)	(1:2)	(1:1)	(2:1)
ρ/kg·m^{-3}	298.15	928.72	939.42 0.96·10^3[a]	–	918.11	929.83 0.91·10^3[a] 930.1[b]	–
	313.15	916.82	927.53	938.09	906.59	918.21/ 918.6[b]	930.60
u/m·s^{-1}	298.15	1342.97	1362.79	–	1362.29	1374.37	–
	313.15	1291.04	1311.23	1330.96	1310.08	1323.80	1337.53
$C_{p,m}$/J·mol^{-1}·K^{-1}	298.15	298	283	–	333	317	–
	313.15	310	293	301	344	327	334
n_D	298.15	1.45779	1.47336	–	1.45913	1.47273	–
	313.15	1.45147	1.46695	1.48238	1.45291	1.46637	1.48087
ε	298.15	3.427	3.902	–	3.283	3.635	–
	313.15	3.365	3.782	4.012	3.214	3.540	3.862
γ/mN·m^{-1}	298.15	29.29	29.58	–	29.71	30.02	–
	313.15	28.43	28.08	29.36	28.64	28.93	29.16
η/mPa·s	298.15	7.820	9.201 10.17[a]	–	11.187	12.030 11.24[a] 12.16[b]	–
	313.15	4.769	5.278	5.745	6.569	6.703 6.78[b]	6.738

[a] Ref. [43].
[b] Ref. [42].

Table 4
Fit parameters (A_Y, B_Y, C_Y) and the regression coefficients, R^2, for the thermophysical properties of the studied thymol-based ESs.

Property	[Thy]ESs	A_Y	B_Y	C_Y	R^2
ρ^a/kg·m^{-3}	[Thy:Oct] (1:2)	1166.47	−0.7973		0.99999
	[Thy:Oct] (1:1)	1175.81	−0.7929		0.99999
	[Thy:Oct] (2:1)	1187.47	−0.7964		0.99993
	[Thy:Dec] (1:2)	1147.06	−0.7679		0.99999
	[Thy:Dec] (1:1)	1161.28	−0.7762		0.99999
	[Thy:Dec] (2:1)	1174.56	−0.7787		0.99996
u^a/m·s^{-1}	[Thy:Oct] (1:2)	2371.81	−3.4498		0.99995
	[Thy:Oct] (1:1)	2379.85	−3.4109		0.99997
	[Thy:Oct] (2:1)	2375.19	−3.3347		1.0000
	[Thy:Dec] (1:2)	2381.30	−3.4193		0.99992
	[Thy:Dec] (1:1)	2380.90	−3.3771		0.99995
	[Thy:Dec] (2:1)	2371.49	−3.3019		1.0000
$C_{p,m}{}^a$/J·mol^{-1}·K^{-1}	[Thy:Oct] (1:2)	65.608	0.77908		0.99962
	[Thy:Oct] (1:1)	79.685	0.68277		0.99943
	[Thy:Oct] (2:1)	93.777	0.66294		0.99777
	[Thy:Dec] (1:2)	117.425	0.72281		0.99925
	[Thy:Dec] (1:1)	121.088	0.65684		0.99895
	[Thy:Dec] (2:1)	118.163	0.68791		0.99826
$n_D{}^a$	[Thy:Oct] (1:2)	1.58359	$-4.22{\cdot}10^{-4}$		1.0000
	[Thy:Oct] (1:1)	1.60264	$-4.33{\cdot}10^{-4}$		0.99997
	[Thy:Oct] (2:1)	1.62068	$-4.42{\cdot}10^{-4}$		0.99997
	[Thy:Dec] (1:2)	1.58285	$-4.15{\cdot}10^{-4}$		0.99999
	[Thy:Dec] (1:1)	1.59887	$-4.23{\cdot}10^{-4}$		0.99997
	[Thy:Dec] (2:1)	1.61882	$-4.40{\cdot}10^{-4}$		0.99994
ε^b		7.40	−0.021	$2.75{\cdot}10^{-5}$	0.990

Table 4 (*continued*)

Property	[Thy]ESs	A_Y	B_Y	C_Y	R^2
	[Thy:Oct] (1:2)	11.13	−0.040	$5.28{\cdot}10^{-5}$	0.998
	[Thy:Oct] (1:1)	15.25	−0.062	$8.43{\cdot}10^{-5}$	0.999
	[Thy:Oct] (2:1)	6.23	−0.015	$1.80{\cdot}10^{-5}$	0.9974
	[Thy:Dec] (1:2)	8.27	−0.024	$2.93{\cdot}10^{-5}$	0.99997
	[Thy:Dec] (1:1)	8.09	−0.020	$2.00{\cdot}10^{-5}$	0.99959
	[Thy:Dec] (2:1)				
γ^a/mN·m^{-1}	[Thy:Oct] (1:2)	52.94	−0.079		0.99973
	[Thy:Oct] (1:1)	52.98	−0.078		0.99978
	[Thy:Oct] (2:1)	53.09	−0.076		0.99948
	[Thy:Dec] (1:2)	52.37	−0.076		0.99993
	[Thy:Dec] (1:1)	51.52	−0.072		0.99929
	[Thy:Dec] (2:1)	53.78	−0.078		0.99983
η^c/mPa·s	[Thy:Oct] (1:2)	0.05034	696.30	160.24	0.99997
	[Thy:Oct] (1:1)	0.05015	650.67	173.42	0.99999
	[Thy:Oct] (2:1)	0.07566	502.24	197.18	0.99999
	[Thy:Dec] (1:2)	0.05594	712.75	163.61	0.99999
	[Thy:Dec] (1:1)	0.05924	645.59	176.62	1.0000
	[Thy:Dec] (2:1)	0.05554	612.18	185.57	1.0000

$^aY = A_Y + B_Y T$. $^bY = A_Y + B_Y T + C_Y T^2$. $^cY = A_Y \exp[B_Y/(T - C_Y)]$;$A_\eta$/mPa·s $= \eta_\infty$.

range of concentrations and temperatures studied in this study. The mean relative deviation between the organic and aqueous phases, an issue that must be considered for processes where liquid–liquid equilibrium is involved, was greater than 5%, which ensures good phase separation [40]. The density increased with increasing x_{Thy} because of increased intermolecular interactions. On the other hand, ρ decreased as the length of the aliphatic chain in the acid increased because of the increase in steric hindrance and increase in temperature as a result of the thermal motion (Fig. 3). The isobaric thermal expansibility, $\alpha_p = -(\partial \ln\rho/\partial T)_p$, quantifies this last effect. The difference between α_p values for all mixtures was within the calculated uncertainty, which indicates that the influence of the temperature on density was similar for all mixtures (Table S10). Thus, we can provide a single value for this derived property: α_P=0.853 (±0.04) kK^{-1}. In the literature [44], there are density data for the mixtures of [Thy:Oct] at $x_{Thy} = 0.473$ and [Thy:

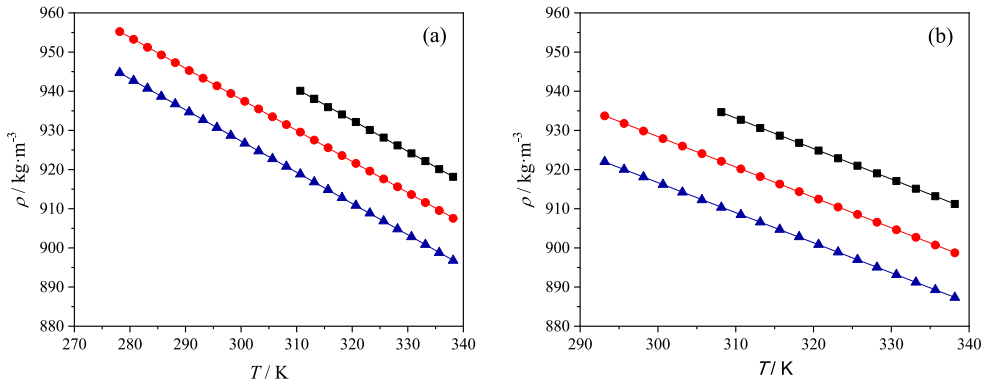

Fig. 3. Density, ρ, of Thy-based ESs at several temperatures, T, and compositions: (▲), (1:2); (●), (1:1); (■), (2:1) in molar ratio. Systems: (a) [Thy:Oct]; (b) [Thy:Dec]. Symbols, experimental values; lines, correlated data.

Dec] at $x_{Thy} = 0.500$. Fig. S2 shows that the literature ρ values were lower than ours for the first system. However, the densities of the mixture with decanoic acid matched very well: $MRD(\rho) = 0.04\%$. Data from Li et al. [45] have not been included in the figure because they are very different from the others (Table 3).

Concerning the speed of sound, the measured values were much lower than those of the hydrophilic eutectic mixtures [30–34]. This fact is in accordance with the weak interactions already deduced from the SLE because a less compact fluid propagates sound at lower speeds than more compact fluids. Thus, an increase in the temperature will also cause a decrease in these values, as can be seen in Fig. S3. From ρ and u, we calculated the compression capacity under isentropic conditions, $\kappa_s = 1/\rho u^2$, and the intermolecular free length, $L_f = K\sqrt{\kappa_s}$, where $K = f(T)$is the Jacobson's constant [61]. The values are listed in Table S10 and range from 510.85 to 766.21 (±0.25) TPa^{-1} and from 0.431 to 0.587 (±0.005) Å, respectively. L_f increased with both the temperature and carboxylic acid molar ratio because both factors weakened the interactions. Otherwise, the steric size of the acid barely influenced L_f.

The amount of heat stored by a pure compound or mixture with increasing temperature, C_p, is less than the amount absorbed in the solid-to-liquid phase change process. However, this property must be explored at different temperatures if that material is to be used as a PCM. The measured values for the [Thy:Dec] system were higher than those for [Thy:Oct], but they were slightly lower than those for eutectic binary mixtures of fatty acids [62]. In addition, concerning the ability to absorb heat, we obtained a linear increase with temperature (Fig. S4).

We modelled the three above properties with PC-SAFT EoS according to the methodology described in Section 2.4.2, and the results, in terms of mean relative deviations, are reported in Table S7. For all mixtures, the model slightly overpredicted the density values (Fig. S5a) and the average deviations for [Thy:Oct] and [Thy:Dec] were$\overline{MRD}(\rho) = 0.99\%$ and 0.82%, respectively. The u and C_p values are obtained as second-order derivative thermodynamic properties, and therefore, they accumulate several errors in the calculation. The speed of sound depends on the ratio between isobaric and isochoric heat capacities (C_p/C_p) and on the variation of the pressure with the density ($\partial p/\partial\rho$). Therefore, the deviations in the speed of sound are mainly due to the $p-\rho$ relation because some errors in the heat capacity estimation are cancelled. The average deviations were $\overline{MRD}(u) = 4.08\%$ for [Thy:Oct] and 6.49% for [Thy:Dec]. In addition, no clear trends were observed (Fig. S5b). Otherwise, in the expression for C_p are included both ($\partial p/\partial\rho$) and ($\partial p/\partial T$) derivatives so that higher deviations and some trend with the temperature can be expected. Indeed, for the [Thy:Oct] system, the deviations increased sharply with increasing temperature (Fig. S5c), and the average value was the highest, $\overline{MRD}(C_{p,m})$ at 23%. For [Thy:Dec], the influence of temperature was less pronounced (Fig. S5c) and $\overline{MRD}(C_{p,m})$ = 10%. Some authors have improved the prediction of these properties with this model by modifying the values of the universal constants of the dispersion term (Eqs. (6) and (7)) [63]. However, more studies on this are necessary.

The refractive index can be used to evaluate the packing of fluids owing to the less compact fluid structure and the higher the speed of light through the material, and, consequently, lower refractive index. Our results were in agreement with the compressibility data and, thus, the n_D values decreased with increasing motion thermal (Fig. S6). The refraction index and density data allow the estimation of the free volume (f_m) that quantifies the packing of the molecules within the fluid. This quantity was calculated by subtracting the molar volume (V_m) from the molar refraction (R_m) because the latter is associated with the hard core volume of a mole of molecules [64]. We obtained the molar refraction with the Lorentz–Lorentz relation, $R_m = V_m(n_D^2-1)/(n_D^2+2)$, and the values slightly increased with T and more sharply with the length of the chain. For [Thy:Dec], R_m ranged from 48.171 to 49.225 (±0.004) $cm^3{\cdot}mol^{-1}$ and f_m from 121.14 to 136.62 (±0.03) $cm^3{\cdot}mol^{-1}$. These values were, on average, 10% higher than for the other system (Table S10). Despite this, the percentage of free volume was similar for all mixtures, f_m/V_m=72.4%.

The experimental values of the static permittivity are useful for analysing the structure of polar fluids. We estimated the orientation of the dipoles in our mixtures using the equation derived by Fröhlich [65]:

$$g\mu^2 = \frac{9kT\varepsilon_0 V_m}{N_A}\frac{(\varepsilon - n_D^2)(2\varepsilon + n_D^2)}{\varepsilon(n_D^2+2)^2}, \quad (12)$$

where g is the Kirkwood–Fröhlich correlation parameter; k, the Boltzmann constant; T, the temperature in Kelvin; ε_0, the vacuum static permittivity; N_A, the Avogadro number; and V_m, ε, n_D and μ are the molar volume, the static permittivity, the refraction index, and the dipole moment of the fluid, respectively at temperature T. The g factor indicates the relative orientation of the neighbouring dipoles. Liquids with parallel preferential disposal between dipoles have $g > 1$. In contrast, the value for a fluid with antiparallel dipoles is lower than unity. For mixtures, the dipole moment is estimated from that of the pure components $\mu^2 = x_1\mu_1^2 + x_2\mu_2^2$. In the literature [66,67], we found μ data for Thy and Oct (Table S1) and calculated the g parameter for the [Thy:Oct] system, which ranged from 0.90 to 1.32. For the lower thymol composition, the preferred orientation between dipoles was antiparallel, as in the pure carboxylic acids [68]. In contrast, it was parallel for $x_{Thy} \geq 0.5$. No μ_{Dec} was found. On the basis that the μ_i values for several substances are not available, the polarisation can be also discussed in terms of the product $g\mu^2$, the so-called orientational dipolar parameter. Table S10 lists the $g\mu^2$ values calculated for both systems at each temperature, and Fig. 4a displays these data at T = 338.15 K and those reported in the literature for pure Thy and Oct [68]. It can be seen that the increase in the length of the acid chain hardly affected the dipole

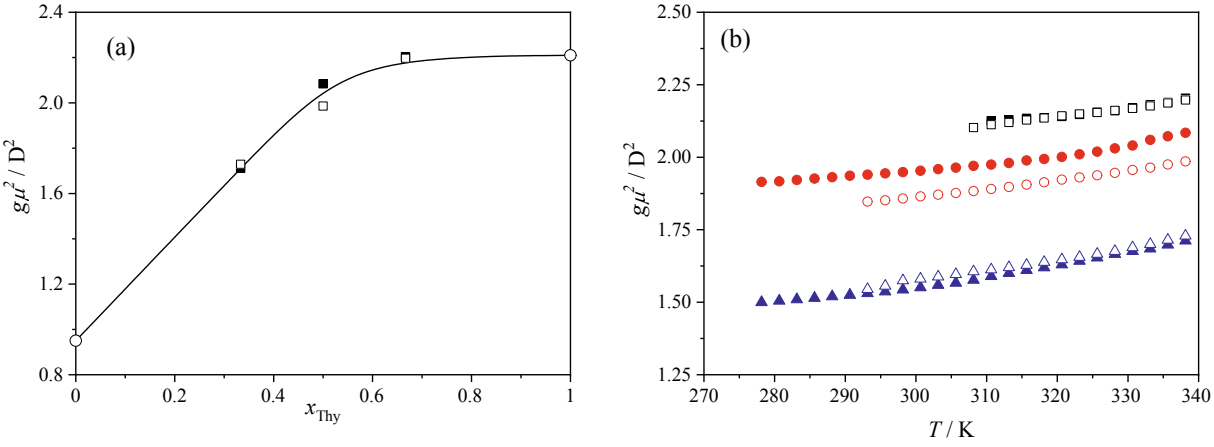

Fig. 4. (a) Orientational dipolar parameter, $g\mu^2$, at$T = 338.15$ K as a function of the thymol molar ratio, x_{Thy}. (□), [Thy:Oct]; (■), [Thy:Dec]; (○), Ref. [68]; (b) $g\mu^2$, as a function of the temperature, T. Full symbols, [Thy:Oct]; empty symbols, [Thy:Dec]. (▲), (1:2); (●), (1:1); (■), (2:1) in molar ratio.

behaviour of the mixtures. For the compositions greater than 0x_{Thy}.6, the orientation of the dipoles was similar to that of pure thymol, which demonstrates the non-additive nature of the $g\mu^2$ factor. The influence of the temperature on the static permittivity is a result of its influence on the refraction index, molar volume, and orientation of the dipoles. This latter seems to be the largest factor, so a similar variation for ε and $g\mu^2$ could be expected. In our study, the static permittivity decreased with increasing temperature (Fig. S7), following a polynomial equation (Table 4). However, the orientational dipolar parameter slightly increased with T (Fig. 4b). This fact was observed for other liquids [68] and was explained as a consequence of the destabilisation of cyclic aggregates by thermal agitation. Therefore, the number of aggregates in the form of a linear chain that exhibits a larger effective dipole increases.

The surface tension characterises the liquid–air interface, so it is related to the droplet formation ability. Low surface tension increases the efficiency of processes in which solvent atomisation is necessary. The measured data for the studied Thy-based ESs ranged from 26.04 to 31.26 mN·m^{-1} and were similar for all mixtures, linearly decreasing with increase in T (Fig. 5). Thus, we can provide average values of the entropy ($\Delta S_S = -(\partial\gamma/\partial T)_p$) and the enthalpy ($\Delta H_S = \gamma - T(\partial\gamma/\partial T)_p$) of the surface per unit surface area of 0.076 ± 0.002 mN·m^{-1}·K^{-1} and 31.4 ± 0.8 mN·m^{-1}, respectively, for both systems. They were much lower than those obtained for hydrophilic eutectics [28–32], indicating that the hydrophobic mixtures form less structured liquids. This result was expected considering the different types of interactions in both ES types.

The critical temperature (T_c) is a necessary parameter in most thermodynamic models, but its experimental measurement is difficult, especially for compounds that undergo thermal degradation. Thus, equations of different formulations are typically collected for the estimation of the critical point [60]. Herein, we used the Li equation [69] to calculate the critical temperature of the mixture from those of the pure compounds. In addition, we applied the PC-SAFT EoS that previously has well predicted both the SLE and volumetric properties of these systems. Finally, we used two equations based on the theory of corresponding states that relate T_c to γ via the Guggenheim equation [70] and with γ and ρ via the work of Eötvos [71]. Both relationships satisfy $\gamma = 0$ at, $T = T_c$ and they have been validated for several ionic liquids [72–74]. We also obtained T_c for the pure compounds with γ and ρ data from the literature [75]. The values and corresponding equations are listed in Table S11. Note that the values of T_c calculated for pure Thy using all equations were higher, from 38 K with PC-SAFT to 79 K using the Eötvos equation, than that reported by Radice in 1899 [75]: T_c= 698.3 K. Considering that thymol exhibits thermal degradation at 433 K [76], perhaps the experimental value should be revised. In addition, the average mean relative deviation for the carboxylic acids was less than 1%. For the mixtures, the T_c data obtained with the Li equation were lower than those obtained with the others owing to the low value for Thy as mentioned above. Assuming that PC-SAFT provides an adequate

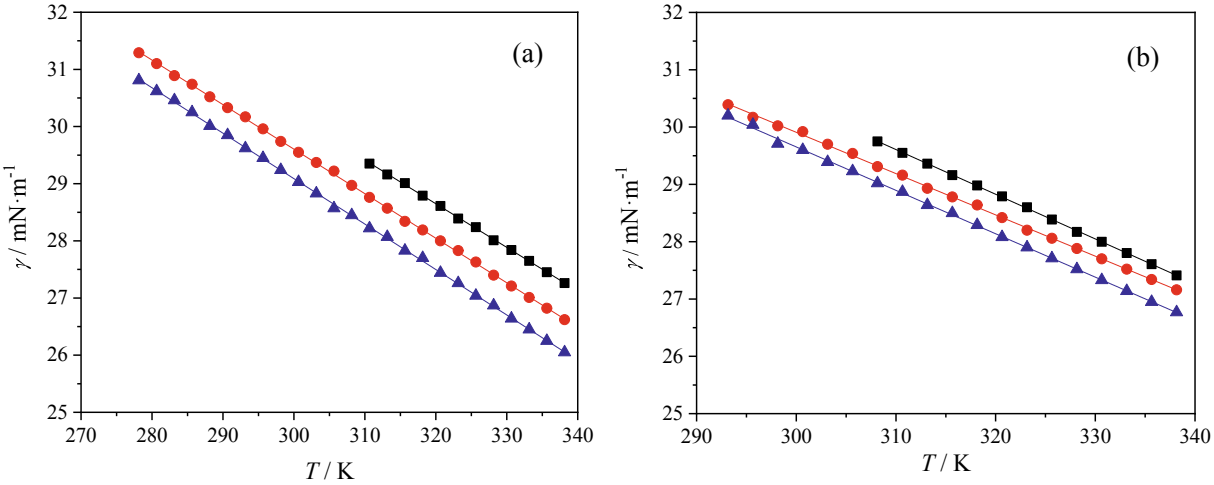

Fig. 5. Surface tension, γ, of Thy-based ESs at several temperatures, T, and compositions: (▲), (1:2); (●), (1:1); (■), (2:1) in molar ratio. Systems: (a) [Thy:Oct]; (b) [Thy:Dec]. Symbols, experimental values; lines, correlated data.

thermodynamic model for our mixtures, the average deviations based on the Guggenheim and Eötvos equations were $\overline{MRD(T_c)} = 4.9\%$ and 7.6%, respectively. Fig. S8 shows the estimated critical locus of the Thy-based ESs.

The fluidity of a substance is a very important property in the design and optimisation of industrial processes. It is a function of the size and shape of the molecules, as well as of the intermolecular interactions. Thus, we calculated the dynamic viscosity (η) of the Thy-based ESs from the experimental density and kinematic viscosity ($\eta = \rho\nu$) data (Tables S8 and S9). Generally, the lower the viscosity value, the better the action of the solvent fluid. Thus, one of the advantages of hydrophobic versus hydrophilic ESs is the greater fluidity of the former. For instance, at 313 K, $\eta = 5.1.10^5$ mPa·s for the choline chloride:citric acid (1:1) mixture [77], whereas the viscosity in this work was 4.772–6.739 mPa·s. We found literature data [44] for [Thy:Oct] mixtures at $x_{Thy} = 0.421$ and [Thy:Dec] at $x_{Thy} = 0.500$, and the values are consistent with ours, as shown in Fig. S9, and the deviation for the second mixture was $MRD(\eta) = 1.2\%$. Again, the data of Li et al. [45] are not included in the figure because they do not match with the other reported data (Table 3). Fluidity is favoured by thermal motion, especially at low T (Fig. 6), so η varies exponentially, $\eta = A_\eta \exp(B_\eta/(T - C_\eta))$. The fit parameters ($A_\eta$, B_η, and C_η) are listed in Table 4. The first is the viscosity at infinite temperature, so the fluidity is only conditioned by steric constraints. The other coefficients are related to the energy barrier that must be overcome for a molecule to move around others, $E_{a,\eta} = R\partial(\ln\eta)/\partial(1/T)$. At 313.15 K, the flow viscous energy ranged from 23.52 to 29.95 kJ mol^{-1}. The values increased (Fig. 7) with increase in thymol molar ratio because of the increased interactions and were larger for the [Thy:Dec] system because of the higher steric hindrance. Using our experimental data, we have correlated $\eta and \gamma$ using the Pelofsky and Murkerjee equations, which have already been validated for several types of fluids [72,78,79]. The expressions and fit coefficients are reported in Table S12. The linearity of the logarithmic fitting ($R^2 > 0.97$) suggests good agreement, better than that proposed by Pelofsky, for both correlations.

In summary, the difference of densities between water and [Thy]ESs and the low viscosity values of the latter will allow a good phase separation and mass transfer in the extraction process evaluated below. Also, the density, refraction index, and the static permittivity have provided the orientational dipolar parameter of these mixtures which is related to their solvent capability.

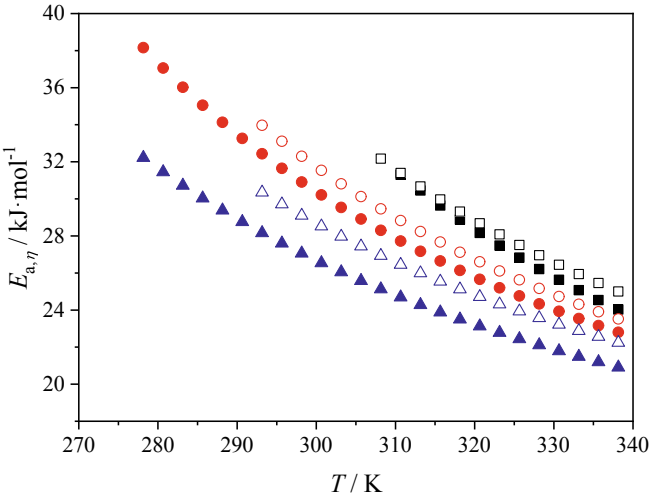

Fig. 7. Flow viscous energy, $E_{a,\eta}$, at several temperatures, T, and compositions: (▲), (1:2); (●), (1:1); (■), (2:1) in molar ratio. Full symbols, [Thy:Oct] system; empty symbols, [Thy:Dec] system.

3.3. Solubility and extraction efficiency

In this section, the aqueous solubilities (W_x) of several poorly water-soluble compounds (quercetin (*Q*), nitrofurantoin (*NF*), and tetracycline (*TC*)) and in the thymol-based eutectic mixtures are presented. Furthermore, the capability of the Thy-based ESs to extract these substances from water is evaluated.

Bioavailability is defined as the fraction of an orally administered substance that is absorbed and available for physiological activity or storage [80]. In practice, this pharmacological concept is calculated from the amount of drug in the plasma. It is strongly related to the solubility of the compound in the administered form, and several factors (such as food intake and biliary excretion) contribute to its variability. The published bioavailability values for *Q* [81] and *TC* [82] are 16% and 70%, respectively, and for *NF*, the plasma concentration is very low (<1 mg/L for an oral dose of 100 mg) [83]. Many drugs are poorly soluble in aqueous solutions, so the development of new solvents could improve pharmacokinetic parameters.

From Table 5, we can classify *Q* and *NF* as insoluble substances in water and *TC* as very slightly soluble [84]. The solubility of a solute is determined by its affinity for the solvent. Considering the structures of the components of our systems (Fig. 1), the main solute–solvent

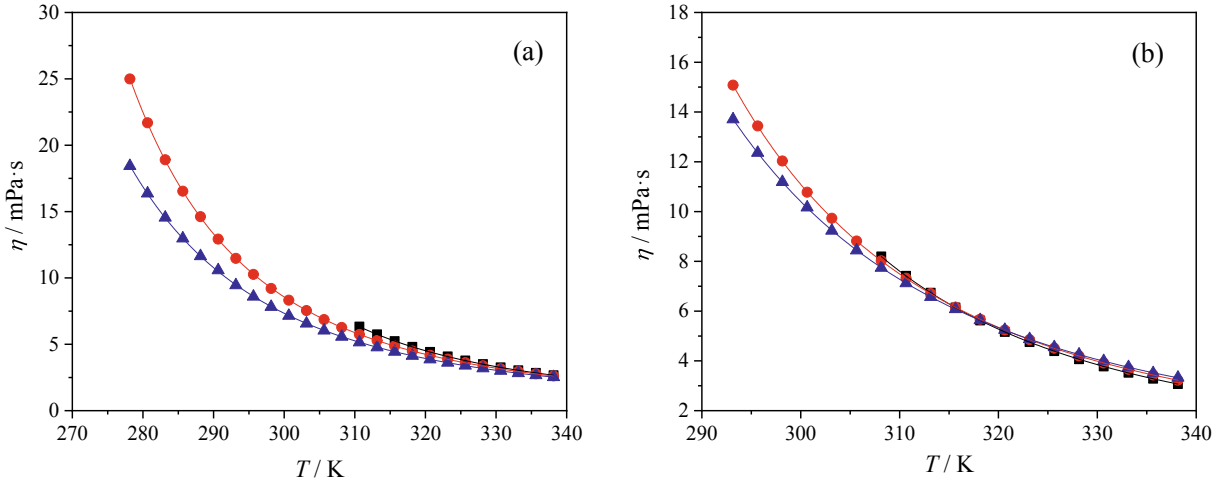

Fig. 6. Dynamic viscosity, η, of Thy-based ESs at several temperatures, T, and compositions: (▲), (1:2); (●), (1:1); (■), (2:1) in molar ratio. Systems: (a) [Thy:Oct]; (b) [Thy:Dec]. Symbols, experimental values; lines, correlated data.

Table 5
Solubility ($W_i = g_i/g_{solvent}$) at $T = 298.15$ K, of quercetin (*Q*), nitrofurantoin (*NT*), and tetracycline (*TC*), in water and in the studied thymol-based ESs.

Thymol-based ESs	W_Q	W_{NT}	W_{TC}
Water	$(2.3 \pm 0.2)\cdot10^{-7}$ $1.61\cdot10^{-7}$ [a] $4.3\cdot10^{-7}$ [d]	$(8.1 \pm 0.4)\cdot10^{-5}$ $7.94\cdot10^{-5}$[b]	$(7.6 \pm 0.6)\cdot10^{-4}$ $4.40\cdot10^{-4}$[c] $1\cdot10^{-4}$ [e]
[Thy:Oct] (1:2)	$(1.89 \pm 0.07)\cdot10^{-4}$	$(2.40 \pm 0.04)\cdot10^{-4}$	0.094 ± 0.007
[Thy:Oct] (1:1)	$(1.81 \pm 0.06)\cdot10^{-4}$	$(4.39 \pm 0.05)\cdot10^{-4}$	0.155 ± 0.009
[Thy:Dec] (1:2)	$(1.38 \pm 0.02)\cdot10^{-4}$	$(1.67 \pm 0.03)\cdot10^{-4}$	0.100 ± 0.003
[Thy:Dec] (1:1)	$(1.72 \pm 0.03)\cdot10^{-4}$	$(3.66 \pm 0.06)\cdot10^{-4}$	0.074 ± 0.004

[a] $T = 289.15$ K, Ref. [86]; [b] $T = 298.1$ K, Ref. [87]; [c] $T = 298.15$ K, Ref. [85]; [d] $T = 298.15$ K, Ref. [29]; [e] Ref. [88].

interactions are dipole–dipole, hydrogen bonds, and π-stacking. As shown in Table S1 and Fig. 1, *TC* has the largest dipole moment and the highest number of hydrogen bond acceptors and donors. On the other hand, *Q* has the smallest μ, a high ability to establish H-bonds, and the largest number of π–π interactions. The aqueous solubility sequence is$W_Q < W_{NF} < W_{TC}$, which is consistent with the order of their dipole moments, so this type of interaction seems to be dominant. There is a significant scattering in the published data for W_Q [29,84–86], and our value is consistent with the two newest values. For *NF*, the solubility obtained in this work matches that published by Domanska et al. [88]. Finally, the value of W_{TC} determined by us was higher than that from the literature [86,89]. This may be a result of the storage time, light exposure, or solution acidity, which can cause *TC* decomposition [90].

Eutectic mixtures have shown their usefulness in the design of drug delivery systems both as reaction media and vehicles for poorly soluble active compounds; however, to date, studies have mainly focused on hydrophilic solvents [91]. Herein, we evaluated the ability of hydrophobic Thy-based ESs to dissolve the three studied drugs at 298.15 K. The results obtained for each eutectic mixture (Table 5 and Fig. 8a) reveal a similar order to that found in water, but the values are significantly greater. In particular, W_Q was dramatically increased, although to a lesser extent than in some choline chloride-based DESs previously studied by us [30,31]. The solubility data were similar for all hydrophobic mixtures, which indicates that there are no dominant interactions. Compared to that in an aqueous system, we obtained an enhancement of up to 822-times. In addition, W_{NF} and W_{TC} were different in the several mixtures. For *NF*, we found the highest value for the [Thy:Oct] (1:1) mixture, and this sequence coincides with that for the orientational dipole parameter of the solvents. This order of the dipole–dipole interactions in *NF*–[Thy] ES systems is in accordance with the lower ability of this compound to establish both H-bonds and π-stacking interactions. For *TC*, we also obtained the highest solubility for the most polar solvent. In the other mixtures, the sequence showed an increase in solubility with increase in the acid molar ratio; that is, with the larger contribution of the hydrogen bonds.

The presence of drugs in aqueous ecosystems has become a serious environmental issue. Most are excreted in the urine and faeces in high concentrations. Therefore, sewage cleaning mechanisms must be implemented. Following green chemistry principles, these methods should be simple, economical, and eco-friendly. Fortunately, liquid–liquid extraction with eutectic solvents is in accordance with these principles. We analysed the ability of the Thy-based ESs to extract each drug from dilute aqueous solutions at 298.15 K with concentrations of $C_i(Q) = 6\mu$ M, $C_i(NF) = 50\mu$ M, and $C_i(TC) = 75\mu$ M. The full extraction efficiency (*EE*) results are given in Table S13 and Fig. 8b and were $EE(Q) = 89.4$–97.8%, $EE(NF) = 76.2$–84.9%, and $EE(TC) = 78.9$–95.0%. In all cases, [Thy:Oct] (1:1) was the best extraction solvent. We also calculated the average value of the distribution coefficient Thy-based ES–water ($D_{[Thy]ESs/w}$) for each drug (Table S13). For *Q* and *TC*, the results were similar to those reported in the literature for octanol–water [92,93]; for *NF*, no data were found. Finally, we determined the *EE* carrying out the extraction in three cycles using the most effective mixture, and a sample containing contaminants was subjected to extraction with a volume of [Thy:Oct] (1:1), and the residual aqueous phase was treated with another quantity of fresh solvent, then repeating the process a third time. The final water analysis showed no signal for quercetin ($EE \approx 100\%$), and the efficiencies for *NF* and *TC* were 99.1% and 99.0%, respectively. Considering the measured values of the water content in the DESs (Table S13) and the partition coefficients of Thy ($\log P_{ow} = 3.30$) [94] and Oct and Dec ($\log P_{ow} = 3.05$ and 4.09, respectively) [95], exchange between phases in the extraction process could be considered negligible. Anyway, we measured the quantity of remaining thymol in water after extraction took place by UV–VIS and the value, 0.97 mg/g, was similar to that reported in the literature [86]. It should be note that the Environmental Protection Agency has eliminated the need to establish a maximum permissible level for thymol residues because it considers it a compound with minimal toxicity [96]. Therefore, the contamination of the water by thymol is much less important than that by the drugs. The organic phase could be treated with activated carbon to recycle it by separating the solute without leaving solid residues in the aqueous phase [39].

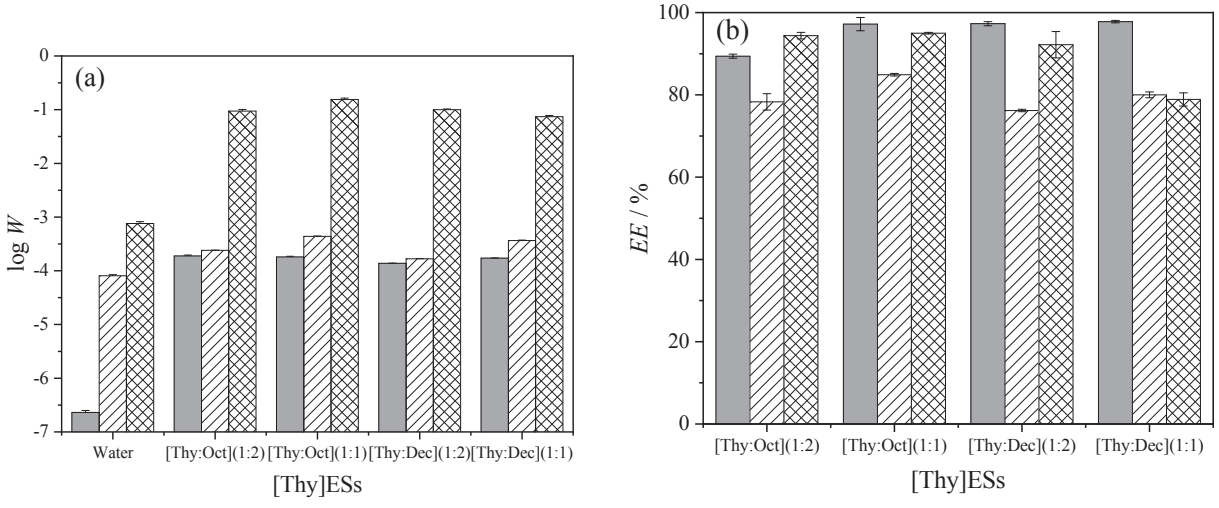

Fig. 8. (a) Solubility of several drugs in water and in the eutectic mixtures. (b) Extraction efficiency of the [Thy]ESs to removal drugs from water. $T = 298.15$ K; 1 cycle. (▓), *Q*; (▨), *NF*; and (▩), *TC*.

4. Conclusions

In this study, we determined the solid–liquid equilibria of two hydrophobic eutectic systems composed of thymol and octanoic or decanoic acid: [Thy:Oct] and [Thy:Dec], respectively. For mixtures close to the eutectic point, we measured and correlated several thermodynamic and transport properties (density, speed of sound, isobaric molar capacity, refraction index, static permittivity, surface tension, and kinematic viscosity) at temperatures up to 338.15 K and a pressure of $p = 0.1$ MPa. From these values, we calculated other properties such as the intermolecular free length, orientational dipolar parameter, enthalpy and entropy of the surface, critical temperature, and activation energy of the fluid viscous. We also used the PC-SAFT EoS to model the SLE, ρ, u, and $C_{p,m}$. Once the solvents had been characterised, we analysed their ability to dissolve three poorly soluble drugs in water, as well as their power to extract these compounds (quercetin, nitrofurantoin, and tetracycline) from contaminated water.

From the thermophysical characterisation, we found that both systems presented a slight negative deviation from ideality. Their densities were lower than that of water, ensuring good phase separation in the extraction processes in aqueous media. Further, the mixtures were less compact with increasing acid concentration and chain length. The heat capacities of the mixtures were slightly lower than that of the carboxylic acid eutectic mixtures, whereas the values of the surface tension and viscosity were moderate, making them suitable for industrial operation. Moreover, we found an antiparallel preferred orientation of the dipoles at lower thymol concentrations and parallel orientation at higher ones. We also observed destabilisation of the cyclic aggregates by thermal agitation. With respect to the final goal of this study, the solubility of the drugs in the studied hydrophobic mixtures was higher than that in water, especially for *Q* (up to 822-times) in which no dominant interaction was detected. For *NF* and *TC*, we obtained the highest solubility (5.4 and 204-fold, respectively) for the most polar solvent: [Thy:Oct] (1:1) mixture. Again, we obtained the highest extraction efficiency for the most polar solvent, with values of $EE(Q) = 97.8\%$, $EE(NF) = 84.9\%$, and $EE(TC) = 95.0\%$. A three cycle extraction procedure allowed the extraction of more than 99% of the drugs.

An interesting outlook would be to establish a database of the physicochemical properties of ESs as new eco-friendly solvents. Then, the characterization of more mixtures is a remaining work. Also, more experiments about their ability as extractants are needed. Soon, we will extend the type of study carried out in this paper to other eutectic mixtures, both hydrophobic and hydrophilic, ionic and non-ionic.

Declaration of Competing Interest

The authors declare that they have no known competing financial interests or personal relationships that could have appeared to influence the work reported in this paper.

Acknowledgments

PLATON research group acknowledges financial support from Gobierno de Aragón and Fondo Social Europeo “Construyendo Europa desde Aragón” E31_17R as well as from University of Zaragoza (n°23340).

Appendix A. Supplementary data

Supplementary data to this article can be found online at https://doi.org/10.1016/j.cej.2021.128472.

References

[1] Efpia, No Title, (n.d.). https://www.efpia.eu/media/412931/the-pharmaceutical-industry-in-figures-2019.pdf.
[2] H.S. OECD, No Title, (2019). https://stats.oecd.org/Index.aspx?DataSetCode=HEALTH_PHMC.
[3] E.S. of V.A.C. European Medicines Agency, Sales of veterinary antimicrobial agents in 31 European countries in 20, 2019.
[4] F. Desbiolles, L. Malleret, C. Tiliacos, P. Wong-Wah-Chung, I. Laffont-Schwob, Occurrence and ecotoxicological assessment of pharmaceuticals: Is there a risk for the Mediterranean aquatic environment? Sci. Total Environ. 639 (2018) 1334–1348, https://doi.org/10.1016/j.scitotenv.2018.04.351.
[5] Y. Ben, C. Fu, M. Hu, L. Liu, M.H. Wong, C. Zheng, Human health risk assessment of antibiotic resistance associated with antibiotic residues in the environment: a review, Environ. Res. 169 (2019) 483–493, https://doi.org/10.1016/j.envres.2018.11.040.
[6] J. O'Neill, The Review on Antimicrobial Resistance, (2016). amr-review.org/.
[7] C.G. Daughton, T.A. Ternes, Pharmaceuticals and personal care products in the environment: agents of subtle change? Environ. Health Perspect. 107 (suppl 6) (1999) 907–938, https://doi.org/10.1289/ehp.99107s6907.
[8] S.D. Richardson, T.A. Ternes, Water analysis: emerging contaminants and current issues, Anal. Chem. 90 (1) (2018) 398–428, https://doi.org/10.1021/acs.analchem.7b04577.
[9] R.R.Z. Tarpani, A. Azapagic, A methodology for estimating concentrations of pharmaceuticals and personal care products (PPCPs) in wastewater treatment plants and in freshwaters, Sci. Total Environ. 622-623 (2018) 1417–1430, https://doi.org/10.1016/j.scitotenv.2017.12.059.
[10] C.G. Daughton, Cradle-to-cradle stewardship of drugs for minimizing their environmental disposition while promoting human health. II. Drug disposal, waste reduction, and future directions. Environ. Health Perspect. 111 (5) (2003) 775–785, https://doi.org/10.1289/ehp.5948.
[11] M.J. Benotti, R.A. Trenholm, B.J. Vanderford, J.C. Holady, B.D. Stanford, S. A. Snyder, Pharmaceuticals and endocrine disrupting compounds in U.S. Drinking Water, Environ. Sci. Technol. 43 (3) (2009) 597–603, https://doi.org/10.1021/es801845a.
[12] J. Fu, W.-N. Lee, C. Coleman, K. Nowack, J. Carter, C.-H. Huang, Removal of pharmaceuticals and personal care products by two-stage biofiltration for drinking water treatment, Sci. Total Environ. 664 (2019) 240–248, https://doi.org/10.1016/j.scitotenv.2019.02.026.
[13] World Health Organization, Pharmaceuticals in drinking-water, (2012). apps.who.int/iris/handle/10665/44630.
[14] J. Wang, S. Wang, Removal of pharmaceuticals and personal care products (PPCPs) from wastewater: a review, J. Environ. Manage. 182 (2016) 620–640, https://doi.org/10.1016/j.jenvman.2016.07.049.
[15] K.P. Shejale, D. Yadav, H. Patil, S. Saxena, S. Shukla, Evaluation of techniques for the remediation of antibiotic-contaminated water using activated carbon, Mol. Syst. Des. Eng. 5 (4) (2020) 743–756, https://doi.org/10.1039/C9ME00167K.
[16] A. Thirunavukkarasu, R. Nithya, R. Sivashankar, A review on the role of nanomaterials in the removal of organic pollutants from wastewater, Rev. Environ. Sci. Biotechnol. 19 (4) (2020) 751–778, https://doi.org/10.1007/s11157-020-09548-8.
[17] A. Jawed, V. Saxena, L.M. Pandey, Engineered nanomaterials and their surface functionalization for the removal of heavy metals: a review, J. Water Process Eng. 33 (2020) 101009, https://doi.org/10.1016/j.jwpe.2019.101009.
[18] C. Li, S. Yuan, F. Jiang, Y. Xie, Y. Guo, H. Yu, Y. Cheng, H. Qian, W. Yao, Degradation of fluopyram in water under ozone enhanced microbubbles: kinetics, degradation products, reaction mechanism, and toxicity evaluation, Chemosphere 258 (2020) 127216, https://doi.org/10.1016/j.chemosphere.2020.127216.
[19] L. Charuaud, E. Jarde, A. Jaffrezic, M.-F. Thomas, B. Le Bot, Veterinary pharmaceutical residues from natural water to tap water: sales, occurrence and fate, J. Hazard. Mater. 361 (2019) 169–186, https://doi.org/10.1016/j.jhazmat.2018.08.075.
[20] P. Isosaari, V. Srivastava, M. Sillanpää, Ionic liquid-based water treatment technologies for organic pollutants: current status and future prospects of ionic liquid mediated technologies, Sci. Total Environ. 690 (2019) 604–619, https://doi.org/10.1016/j.scitotenv.2019.06.421.
[21] F. Gao, R. Bai, F. Ferlin, L. Vaccaro, M. Li, Y. Gu, Replacement strategies for non-green dipolar aprotic solvents, Green Chem. 22 (19) (2020) 6240–6257, https://doi.org/10.1039/D0GC02149K.
[22] A.P. Abbott, G. Capper, D.L. Davies, R.K. Rasheed, V. Tambyrajah, Novel solvent properties of choline chloride/urea mixtures, Chem. Commun. 9 (2003) 70–71, https://doi.org/10.1039/b210714g.
[23] E.L. Smith, A.P. Abbott, K.S. Ryder, Deep eutectic solvents (DESs) and their applications, Chem. Rev. 114 (21) (2014) 11060–11082, https://doi.org/10.1021/cr300162p.
[24] Y.H. Choi, J. van Spronsen, Y. Dai, M. Verberne, F. Hollmann, I.W.C.E. Arends, G.-J. Witkamp, R. Verpoorte, Are natural deep eutectic solvents the missing link in understanding cellular metabolism and physiology? Plant Physiol. 156 (4) (2011) 1701–1705, https://doi.org/10.1104/pp.111.178426.
[25] C. Li, D. Li, S. Zou, Z. Li, J. Yin, A. Wang, Y. Cui, Z. Yao, Q.i. Zhao, Extraction desulfurization process of fuels with ammonium-based deep eutectic solvents, Green Chem. 15 (10) (2013) 2793, https://doi.org/10.1039/c3gc41067f.
[26] Y. Marcus, Gas solubilities in deep eutectic solvents, Monatsh. Chem. 149 (2) (2018) 211–217, https://doi.org/10.1007/s00706-017-2031-8.
[27] T. Altamash, M.S. Nasser, Y. Elhamarnah, M. Magzoub, R. Ullah, H. Qiblawey, S. Aparicio, M. Atilhan, Gas solubility and rheological behavior study of betaine and alanine based natural deep eutectic solvents (NADES), J. Mol. Liq. 256 (2018) 286–295, https://doi.org/10.1016/j.molliq.2018.02.049.
[28] X.-F. Shao, C. Wang, Y.-J. Yang, B. Feng, Z.-Q. Zhu, W.-J. Wang, Y.i. Zeng, L.-W. Fan, Screening of sugar alcohols and their binary eutectic mixtures as phase

change materials for low-to-medium temperature latent heat storage. (I): non-isothermal melting and crystallization behaviors, Energy 160 (2018) 1078–1090, https://doi.org/10.1016/j.energy.2018.07.081.
[29] X. Ge, C. Gu, X. Wang, J. Tu, Deep eutectic solvents (DESs)-derived advanced functional materials for energy and environmental applications: challenges, opportunities, and future vision, J. Mater. Chem. A 5 (18) (2017) 8209–8229, https://doi.org/10.1039/C7TA01659J.
[30] F. Bergua, I. Delso, J. Muñoz-Embid, C. Lafuente, M. Artal, Structure and properties of two glucose-based deep eutectic systems, Food Chem. 336 (2021) 127717, https://doi.org/10.1016/j.foodchem.2020.127717.
[31] N. López, I. Delso, D. Matute, C. Lafuente, M. Artal, Characterization of xylitol or citric acid:choline chloride:water mixtures: Structure, thermophysical properties, and quercetin solubility, Food Chem. 306 (2020) 125610, https://doi.org/10.1016/j.foodchem.2019.125610.
[32] D. Lapeña, L. Lomba, M. Artal, C. Lafuente, B. Giner, The NADES glyceline as a potential Green Solvent: a comprehensive study of its thermophysical properties and effect of water inclusion, J. Chem. Thermodyn. 128 (2019) 164–172, https://doi.org/10.1016/j.jct.2018.07.031.
[33] D. Lapeña, F. Bergua, L. Lomba, B. Giner, C. Lafuente, A comprehensive study of the thermophysical properties of reline and hydrated reline, J. Mol. Liq. 303 (2020) 112679, https://doi.org/10.1016/j.molliq.2020.112679.
[34] D. Lapeña, L. Lomba, M. Artal, C. Lafuente, B. Giner, Thermophysical characterization of the deep eutectic solvent choline chloride:ethylene glycol and one of its mixtures with water, Fluid Phase Equilib. 492 (2019) 1–9, https://doi.org/10.1016/j.fluid.2019.03.018.
[35] I. Delso, C. Lafuente, J. Muñoz-Embid, M. Artal, NMR study of choline chloride-based deep eutectic solvents, J. Mol. Liq. 290 (2019) 111236, https://doi.org/10.1016/j.molliq.2019.111236.
[36] D.J.G.P. Van Osch, L.F. Zubeir, A. Van Den Bruinhorst, M.A.A. Rocha, M.C. Kroon, Hydrophobic deep eutectic solvents: water-immiscible extractants, Green Chem. (2015) 1–36, https://doi.org/10.1039/C5GC01451D.
[37] C. Florindo, L.C. Branco, I.M. Marrucho, Quest for green-solvent design: from hydrophilic to hydrophobic (Deep) eutectic solvents, ChemSusChem 12 (8) (2019) 1549–1559, https://doi.org/10.1002/cssc.201900147.
[38] D.O. Abranches, M.A.R. Martins, L.P. Silva, N. Schaeffer, S.P. Pinho, J.A. P. Coutinho, Phenolic hydrogen bond donors in the formation of non-ionic deep eutectic solvents: the quest for type V DES, Chem. Commun. 55 (69) (2019) 10253–10256, https://doi.org/10.1039/C9CC04846D.
[39] C. Florindo, F. Lima, L.C. Branco, I.M. Marrucho, Hydrophobic deep eutectic solvents: a circular approach to water purification, ACS Sustain. Chem. Eng. (2019), https://doi.org/10.1021/acssuschemeng.9b02658.
[40] D.J.G.P. van Osch, C.H.J.T. Dietz, J. van Spronsen, M.C. Kroon, F. Gallucci, M. van Sint Annaland, R. Tuinier, A search for natural hydrophobic deep eutectic solvents based on natural components, ACS Sustainable Chem. Eng. 7 (3) (2019) 2933–2942, https://doi.org/10.1021/acssuschemeng.8b03520.s001.
[41] O.G. Sas, M. Castro, Á. Domínguez, B. González, Removing phenolic pollutants using deep eutectic solvents, Sep. Purif. Technol. 227 (2019) 115703, https://doi.org/10.1016/j.seppur.2019.115703.
[42] G. Almustafa, R. Sulaiman, M. Kumar, I. Adeyemi, H.A. Arafat, I. AlNashef, Boron extraction from aqueous medium using novel hydrophobic deep eutectic solvents, Chem. Eng. J. 395 (2020) 125173, https://doi.org/10.1016/j.cej.2020.125173.
[43] P. Makoś, E. Słupek, J. Gębicki, Hydrophobic deep eutectic solvents in microextraction techniques–a review, Microchem. J. 152 (2020) 104384, https://doi.org/10.1016/j.microc.2019.104384.
[44] M.A.R. Martins, E.A. Crespo, P.V.A. Pontes, L.P. Silva, M. Bülow, G.J. Maximo, E.A. C. Batista, C. Held, S.P. Pinho, J.A.P. Coutinho, Tunable hydrophobic eutectic solvents based on terpenes and monocarboxylic acids, ACS Sustainable Chem. Eng. 6 (7) (2018) 8836–8846, https://doi.org/10.1021/acssuschemeng.8b01203.s001.
[45] K.e. Li, Y. Jin, D. Jung, K. Park, H. Kim, J. Lee, In situ formation of thymol-based hydrophobic deep eutectic solvents: application to antibiotics analysis in surface water based on liquid-liquid microextraction followed by liquid chromatography, J. Chromatogr. A 1614 (2020) 460730, https://doi.org/10.1016/j.chroma.2019.460730.
[46] A. Marchese, I.E. Orhan, M. Daglia, R. Barbieri, A. Di Lorenzo, S.F. Nabavi, O. Gortzi, M. Izadi, S.M. Nabavi, Antibacterial and antifungal activities of thymol: a brief review of the literature, Food Chem. 210 (2016) 402–414, https://doi.org/10.1016/j.foodchem.2016.04.111.
[47] D.E. Goon, S.H.S. Abdul Kadir, N.A. Latip, S.A. Rahim, M. Mazlan, Palm oil in lipid-based formulations and drug delivery systems, Biomolecules 9 (2019) 1–19, https://doi.org/10.3390/biom9020064.
[48] J.-P. Douliez, N. Martin, C. Gaillard, T. Beneyton, J.-C. Baret, S. Mann, L. Beven, Catanionic coacervate droplets as a surfactant-based membrane-free Protocell model, Angew. Chem. Int. Ed. 56 (44) (2017) 13689–13693, https://doi.org/10.1002/anie.201707139.
[49] Y. Yuan, N. Zhang, W. Tao, X. Cao, Y. He, Fatty acids as phase change materials: a review, Renew. Sustain. Energy Rev. 29 (2014) 482–498, https://doi.org/10.1016/j.rser.2013.08.107.
[50] N. Zhang, Y. Yuan, X. Cao, Y. Du, Z. Zhang, Y. Gui, Latent heat thermal energy storage systems with solid-liquid phase change materials: a review, Adv. Eng. Mater. 20 (2018) 1700753, https://doi.org/10.1002/adem.201700753.
[51] H. Sereshti, S. Semnani Jazani, N. Nouri, G. Shams, Dispersive liquid–liquid microextraction based on hydrophobic deep eutectic solvents: application for tetracyclines monitoring in milk, Microchem. J. 158 (2020) 105269, https://doi.org/10.1016/j.microc.2020.105269.
[52] X. Wei, Y. Wang, J. Chen, F. Xu, Z. Liu, X. He, H. Li, Y. Zhou, Adsorption of pharmaceuticals and personal care products by deep eutectic solvents-regulated magnetic metal-organic framework adsorbents: performance and mechanism, Chem. Eng. J. 392 (2020) 124808, https://doi.org/10.1016/j.cej.2020.124808.
[53] V. Antón, H. Artigas, J. Muñoz-Embid, M. Artal, C. Lafuente, Thermophysical study of 2-acetylthiophene: experimental and modelled results, Fluid Phase Equilib. 433 (2017) 126–134, https://doi.org/10.1016/j.fluid.2016.10.026.
[54] J. Gross, G. Sadowski, Perturbed-chain SAFT: an equation of state based on a perturbation theory for chain molecules, Ind. Eng. Chem. Res. 40 (2001) 1244–1260, https://doi.org/10.1021/ie0003887.
[55] J. Gross, G. Sadowski, Application of the perturbed-chain SAFT equation of state to associating systems, Ind. Eng. Chem. Res. 41 (22) (2002) 5510–5515, https://doi.org/10.1021/ie010954d.
[56] H. Renon, J.M. Prausnitz, Local compositions in thermodynamic excess functions for liquid mixtures, AIChE J. 14 (1) (1968) 135–144, https://doi.org/10.1002/aic.690140124.
[57] W.G. Chapman, G. Jackson, K.E. Gubbins, Phase equilibria of associating fluids: Chain molecules with multiple bonding sites, Mol. Phys. 65 (5) (1988) 1057–1079, https://doi.org/10.1080/00268978800101601.
[58] J.A. Barker, D. Henderson, Perturbation theory and equation of state for fluids: the square-well potential, J. Chem. Phys. 47 (8) (1967) 2856–2861, https://doi.org/10.1063/1.1712308.
[59] J.A. Barker, D. Henderson, Perturbation theory and equation of state for fluids. II. A successful theory of liquids, J. Chem. Phys. 47 (11) (1967) 4714–4721, https://doi.org/10.1063/1.1701689.
[60] E.G. Prausnitz, J.M. Lichtenthaler, R.N. Azevedo, Molecular Thermodynamics of the Fluid Phase Equilibria, Prentice-Hall, 1986.
[61] B. Jacobson, Ultrasonic velocity in liquids and liquid mixtures, J. Chem. Phys. 20 (5) (1952) 927–928, https://doi.org/10.1063/1.1700615.
[62] H. Nazir, M. Batool, M. Ali, A.M. Kannan, Fatty acids based eutectic phase change system for thermal energy storage applications, Appl. Therm. Eng. 142 (2018) 466–475, https://doi.org/10.1016/j.applthermaleng.2018.07.025.
[63] X. Liang, B. Maribo-Mogensen, K. Thomsen, W. Yan, G.M. Kontogeorgis, Approach to improve speed of sound calculation within PC-SAFT framework, Ind. Eng. Chem. Res. 51 (45) (2012) 14903–14914, https://doi.org/10.1021/ie3018127.
[64] P. Brocos, Á. Piñeiro, R. Bravo, A. Amigo, Refractive indices, molar volumes and molar refractions of binary liquid mixtures: concepts and correlations, PCCP 5 (2003) 550–557, https://doi.org/10.1039/b208765k.
[65] H. Fröhlich, General theory of the static dielectric constant, Trans. Faraday Soc. 44 (0) (1948) 238–243, https://doi.org/10.1039/TF9484400238.
[66] C.G. Le Fèvre, R.J.W. Le Fèvre, K.W. Robertson, 107. The dipole moments of p-cymene; 2- and 3-halogeno-p-cymenes, carvacrol, and thymol; p-ethyltoluene; p-tert.-butyltoluene, 1 : 3-dimethyl-5-tert.- butylbenzene, tert.-butylbenzene and its p-nitro-derivative, J. Chem. Soc. (1935) 480–488. doi:10.1039/JR9350000480.
[67] No Title, (n.d.). http://www.stenutz.eu/chem/.
[68] R. Bouteloup, D. Mathieu, Predicting dielectric constants of pure liquids: fragment-based Kirkwood–Fröhlich model applicable over a wide range of polarity, PCCP 21 (21) (2019) 11043–11057, https://doi.org/10.1039/C9CP01704F.
[69] P. Li, P.-S. Ma, J.-G. Dai, W. Cao, Estimations of surface tensions at different temperatures by a corresponding-states group-contribution method, Fluid Phase Equilib. 118 (1) (1996) 13–26, https://doi.org/10.1016/0378-3812(95)02836-6.
[70] E.A. Guggenheim, The principle of corresponding states, J. Chem. Phys. 13 (7) (1945) 253–261, https://doi.org/10.1063/1.1724033.
[71] J.L. Shereshefsky, Surface tension of saturated vapors and the equation of eötvös, J. Phys. Chem. 35 (6) (1931) 1712–1720, https://doi.org/10.1021/j150324a014.
[72] H. Ghaedi, M. Ayoub, S. Sufian, A.M. Shariff, B. Lal, The study on temperature dependence of viscosity and surface tension of several Phosphonium-based deep eutectic solvents, J. Mol. Liq. 241 (2017) 500–510, https://doi.org/10.1016/j.molliq.2017.06.024.
[73] N. Rai, E.J. Maginn, Vapor–liquid coexistence and critical behavior of ionic liquids via, (2011) 1439–1443.
[74] F.S. Mjalli, G. Vakili-Nezhaad, K. Shahbaz, I.M. AlNashef, Application of the Eötvos and Guggenheim empirical rules for predicting the density and surface tension of ionic liquids analogues, Thermochim. Acta 575 (2014) 40–44, https://doi.org/10.1016/j.tca.2013.10.017.
[75] W.G. Linstrom, P.J.; Mallard, NIST Chemistry Webbok, NIST Standard Reference Database Number 69, Gaithersburg MD, 20899, 2020. doi:10.18434/T4D303.
[76] M.K. Trivedi, S. Patil, R.K. Mishra, S. Jana, Structural and physical properties of biofield treated thymol and menthol, J. Mol. Pharm. Org. Process Res. 03 (2015), https://doi.org/10.4172/2329-9053.1000127.
[77] I.M. Aroso, A. Paiva, R.L. Reis, A.R.C. Duarte, Natural deep eutectic solvents from choline chloride and betaine – physicochemical properties, J. Mol. Liq. 241 (2017) 654–661, https://doi.org/10.1016/j.molliq.2017.06.051.
[78] A.H. Pelofsky, Surface tension-viscosity relation for liquids, J. Chem. Eng. Data 11 (3) (1966) 394–397, https://doi.org/10.1021/je60030a031.
[79] M. Pierantozzi, G. Di Nicola, Surface tension correlation of carboxylic acids from liquid viscosity data, Fluid Phase Equilib. 482 (2019) 118–125, https://doi.org/10.1016/j.fluid.2018.11.015.
[80] M.J. Jackson, The assessment of bioavailability of micronutrients: introduction, Eur. J. Clin. Nutr. 51 Suppl 1 (1997) S1-2. http://www.ncbi.nlm.nih.gov/pubmed/9023470.
[81] Y. Guo, R.S. Bruno, Endogenous and exogenous mediators of quercetin bioavailability, J. Nutrit. Biochem. 26 (3) (2015) 201–210, https://doi.org/10.1016/j.jnutbio.2014.10.008.
[82] K.N. Agwuh, Pharmacokinetics and pharmacodynamics of the tetracyclines including glycylcyclines, J. Antimicrob. Chemother. 58 (2006) 256–265. doi:10.1093/jac/dkl224.

[83] A. Novelli, E. Rosi, Pharmacological properties of oral antibiotics for the treatment of uncomplicated urinary tract infections, J. Chemother. 29 (sup1) (2017) 10–18, https://doi.org/10.1080/1120009X.2017.1380357.
[84] Pharmacopeia of the United States of America, 32nd revision, and the National Formulary, 27th edition, 2009.
[85] M.H. Abraham, W.E. Acree Jr., On the solubility of quercetin, J. Mol. Liq. 197 (2014) 157–159, https://doi.org/10.1016/j.molliq.2014.05.006.
[86] D.R. Yalkowsky SH, The AQUASOL dATAbASE of Aqueous Solubility, Fifth ed, Tucson, AZ, 1992.
[87] R. Iqbal, Z. Mehmood, A. Baig, N. Khalid, Formulation and characterization of food grade O/W nanoemulsions encapsulating quercetin and curcumin: Insights on enhancing solubility characteristics, Food Bioprod. Process. 123 (2020) 304–311, https://doi.org/10.1016/j.fbp.2020.07.013.
[88] U. Domańska, A. Pobudkowska, A. Pelczarska, Ł. Żukowski, Modelling, solubility and pKa of five sparingly soluble drugs, Int. J. Pharm. 403 (1-2) (2011) 115–122, https://doi.org/10.1016/j.ijpharm.2010.10.034.
[89] F. Najafi, M. Salami-Kalajahi, H. Roghani-Mamaqani, Synthesis of amphiphilic Janus dendrimer and its application in improvement of hydrophobic drugs solubility in aqueous media, Eur. Polym. J. 134 (2020) 109804, https://doi.org/10.1016/j.eurpolymj.2020.109804.
[90] M.A.J. Mohammed-Ali, Stability study of tetracycline drug in acidic and alkaline solutions by colorimetric method, J. Chem. Pharm. Res. 4 (2012) 1319–1326.
[91] S. Emami, A. Shayanfar, Deep eutectic solvents for pharmaceutical formulation and drug delivery applications, Pharm. Dev. Technol. 25 (7) (2020) 779–796, https://doi.org/10.1080/10837450.2020.1735414.
[92] J.A. Rothwell, A.J. Day, M.R.A. Morgan, Experimental determination of octanol−water partition coefficients of quercetin and related flavonoids, J. Agric. Food Chem. 53 (11) (2005) 4355–4360, https://doi.org/10.1021/jf0483669.
[93] L. Leive, S. Telesetsky, W.G. Coleman, D. Carr, Tetracyclines of various hydrophobicities as a probe for permeability of Escherichia coli outer membranes. Antimicrob. Agents Chemother. 25 (5) (1984) 539–544, https://doi.org/10.1128/AAC.25.5.539.
[94] S. Griffin, S.G. Wyllie, J. Markham, Determination of octanol–water partition coefficient for terpenoids using reversed-phase high-performance liquid chromatography, J. Chromatogr. A 864 (2) (1999) 221–228, https://doi.org/10.1016/S0021-9673(99)01009-2.
[95] G. Siti, A.I. Razmah, Partition coefficient, water solubility and aquatic toxicity of short-chain palm fatty acids, J. Oil Palm Res. 27 (2015) 75–81.
[96] EPA, Thymol; Exemption from the Requirement of a Tolerance, in: Fed. Regist. Vol. 4, 2009: pp. 12613–12617.